## Roman CCS White Paper

# Emission-line Diagnostics of Galaxies at Cosmic Noon with the *Roman Space Telescope* High Latitude Spectroscopic Survey

**Roman Core Community Survey:** ☑ High Latitude Wide Area Survey

**Scientific Categories:** galaxies, stellar populations and the interstellar medium

**Additional scientific keywords:** galaxy evolution, galaxy formation, chemical abundances, interstellar medium, H II regions, starburst galaxies, dwarf galaxies, emission line galaxies

**Submitting Author:**
Name: Ash Danehkar
Affiliation: Eureka Scientific, Inc., Oakland, CA 94602-3017
Email: danehkar@eurekasci.com

**Abstract:**
The determination of the physical and chemical properties of galaxies over cosmic time is crucial to comprehending fundamental aspects of galaxy evolution, such as star-formation regulation and metal enrichment. The UV and optical emission-line fluxes originating from galaxies in their rest frames provide valuable insights into the physical characteristics of star formation, metal content, and ionization states within starburst and active galaxies. Over the last decade, there has been growing research using the rest-frame UV and optical lines of distant galaxies redshifted into the near-IR window to trace the chemical evolution of distant galaxies. In the 2020 decade, the High Latitude Spectroscopic Survey (HLSS) with the *Roman Space Telescope* will significantly increase the rest-frame UV and optical data of galaxies over redshift ranges of $z \sim 1$–$2$. This information supplied by deep *Roman* grism HLSS presents a unique opportunity to examine the interstellar medium (ISM) of galaxies during the periods of cosmic history following reionization, including chemical elements, ionizing radiation fields, stellar populations, and kinematics of stellar feedback. The present white paper briefly discusses the applicability of the *Roman* HLSS for conducting research on plasma diagnostics and abundance analysis of the rest-frame diagnostic emission lines from ionized gaseous nebulae and H II regions within active and star-forming galaxies at cosmic noon ($z \sim 1$–$2$).

## 1 *Roman* Ultra Deep Field: deeper than *Hubble* Ultra Deep Field

Current empirical evidence suggests that early galaxies that formed after the period of cosmic darkness ($z > 11$) underwent a gradual transformation into starburst galaxies (Rieke et al. 1980; Weedman et al. 1981; Balzano 1983) during the epoch of reionization ($6 < z < 11$) (see, e.g., Richard et al. 2006). It is widely believed that primeval galaxies are predominantly comprised of neutral hydrogen during their transformation from a state of high neutrality to one of high ionization, ultimately leading to the emergence of Lyman-$\alpha$ emitters (LAEs) at the end of the reionization process. This phenomenon is observed in over half of all galaxies by $z \sim 6$ (e.g., Dijkstra 2014; Hayes 2015). Subsequently, these galaxies evolve into Lyman-break galaxies (LBGs) following reionization that is completed at around $z \sim 6$ (e.g., Giavalisco 2002). Empirical evidence indicates that the transition into starburst galaxies reached its culmination at a redshift of about 6, coinciding with a significant rise in the neutral fraction of the IGM (see Becker et al. 2015). After reionization, galaxies underwent active phases of star formation and the growth of supermassive black holes (Heckman et al. 1997; González Delgado et al. 1998). It is likely that they may eventually transition into quiescent galaxies by cosmic noon ($z \sim 2$–3) (Gobat et al. 2012; Glazebrook et al. 2017). Quiescent galaxies refer to a group of galaxies that are currently expanding and are typically observed within the redshifts between 1 and 4. These galaxies exhibit multiwavelength photometries that are indicative of a significant reduction in star formation activity (Straatman et al. 2016; Feldmann et al. 2016; Gómez-Guijarro et al. 2018; Belli et al. 2019).

The deepest field that has been acquired to date is the *Hubble* Ultra Deep Field (HUDF; Beckwith et al. 2006) made using the Advanced Camera for Surveys (ACS) in the optical band (Beckwith et al. 2006; Oesch et al. 2007), and the Wide Field Camera 3 (WFC3) in the near-infrared band (Oesch et al. 2010; Ellis et al. 2013; Koekemoer et al. 2013; Illingworth et al. 2013) on the *Hubble Space Telescope* (*HST*). The *HST* was also used in the UV band to further expand the depth of the HUDF (Teplitz et al. 2013; Rafelski et al. 2015). These observations have provided significant insights into the evolution of the faint end of the UV luminosity function (Trenti et al. 2010; Oesch et al. 2013; Bouwens et al. 2014; Finkelstein et al. 2015), the escape fraction of Lyman radiation in high-z galaxies (Tilvi et al. 2014; Rutkowski et al. 2016; Bagley et al. 2017), evolution of the sizes and morphologies of galaxies (Ono et al. 2013; Curtis-Lake et al. 2016; Oesch et al. 2018), and their possible role in cosmic reionization (see, e.g. Trenti et al. 2010; Finkelstein et al. 2012; Robertson et al. 2013; Tilvi et al. 2014). The HUDF has attained the highest possible observational depth for the *HST*, using enormous orbital hours. To further advance the observational depth, the *Hubble* Frontier Fields program (HFF; Lotz et al. 2017) utilized gravitational lensing in six massive lensing cluster fields, which allowed for a ten-fold increase in depth into the luminosity function at redshifts of 8–11 (e.g., Kawamata et al. 2016; Limousin et al. 2016; Priewe et al. 2017; Mahler et al. 2018; Vega-Ferrero et al. 2019). However, the limited HFF coverage resulted in significantly small high-z galaxies being studied.

One of the limitations of the HUDF pertains to their spatial coverage, which is about 2–3 arcmin in diameter, which hinders the possibility of conducting investigations on large-scale clusters of distant faint galaxies. Addressing this limitation is imperative to enhance our comprehension of cosmic reionization and the evolution of galaxies. The *James Webb Space Telescope* (*JWST*) is expected to conduct investigations at greater depths, albeit within the similar spatial coverage. Although larger surveys using the *HST* have been conducted, they often sacrifice depth for area due to the limitations of observing orbits. The combined GOODS (Giavalisco et al. 2004) and

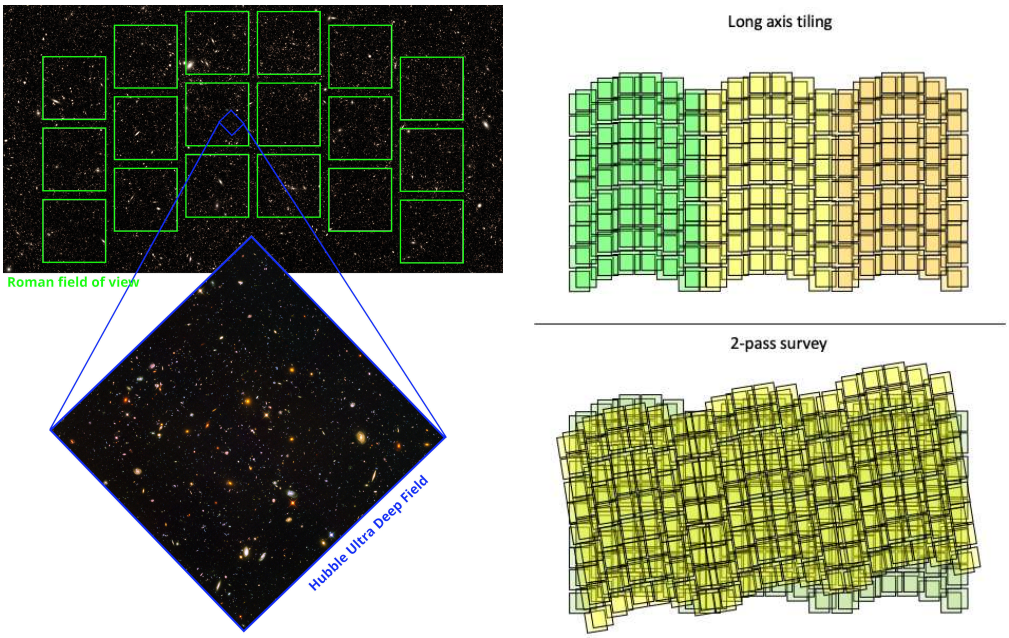


**Figure 1:** *Left Panel:* Field of view of the Wide Field Instrument (WFI) on the *Roman Space Telescope* in comparison to the near-infrared Hubble Ultra Deep Field (HUDF) made with the Wide Field Camera 3 (WFC3) mounted on the synthetic *Roman* ultra-deep field made by Drakos et al. (2022). *Right Panel:* Possible tiling mosaics of the High Latitude Spectroscopic Survey (HLSS) with the *Roman Telescope* covering larger areas (Wang et al. 2022).

CANDELS surveys (Grogin et al. 2011; Koekemoer et al. 2011) offered the coverage of about 30-800 arcmin$^2$ in 10 bandpasses, while the COSMOS survey (Koekemoer et al. 2007; Scoville et al. 2007) spans around 1.6–27 square degrees. They have facilitated investigations into the formation of galaxies at intermediate redshifts at cosmic noon (Ono et al. 2013; Curtis-Lake et al. 2016; Oesch et al. 2018), as well as the brighter end of the luminosity function up to $z \sim 6$–8 (Trenti et al. 2010; Oesch et al. 2013; Bouwens et al. 2014; Finkelstein et al. 2015). Nonetheless, due to the spatial and magnitude limitations, the scope of the research is confined to the exceptionally luminous portion of the luminosity function and the evolution of galaxies at lower redshifts. In order to make substantial progress in our understanding of distant galaxies and reionization, it is imperative to acquire deep images and spectroscopic measurements with qualities comparable to those of the HUDF, but with a coverage area 100 times higher than that of current surveys. This can be achieved through the use of the Wide Field Instrument (WFI) on the *Roman Space Telescope*, as illustrated in Fig. 1.

## 2 High Latitude Spectroscopic Survey: Galaxy Redshift Surveys

The recent technological advancements in near-IR detectors have enabled future missions to study cosmic reionization and the evolution of galaxies. The main objective of the *Nancy Grace Roman Space Telescope*, formerly called the Wide Field Infrared Survey Telescope (WFIRST), is to facilitate a high galactic latitude, large-area slitless spectroscopic survey to map extensive areas of galaxies at $z > 1$. It has been proposed to use the capabilities of the *Roman* mission for conducting the High Latitude Spectroscopic Survey (HLSS; Wang et al. 2022) using the near-IR grism (1.0–1.93 $\mu$m, $R \sim 650$) and the 0.28 deg$^2$ wide-field camera (see Fig. 1), and the High Latitude Imaging Survey (HLIS; e.g., Troxel et al. 2021; Yamamoto et al. 2023). The HLSS could

map 2000 deg$^2$, which offer H$\alpha$ spectroscopic surveys of around 10 million galaxies at $z = 1$–2 and [O III] emission-line measurements of 2 million galaxies at $z = 2 - 3$. Assuming the same areas observed by the HLSS will also be recorded by the HLIS, it could also conduct high-angular resolution imaging of galaxies for constructing their spectral energy distributions (SEDs). The H$\alpha$ survey would facilitate accurate measurements of the distance-redshift relation and the $H(z)$ expansion rate for proper constraints on cosmic acceleration (see, e.g., Frieman et al. 2008; Caldwell & Kamionkowski 2009; Weinberg et al. 2013). Additionally, the *Roman* survey would enable precise measurements of the growth of dark matter clustering through redshift-space distortions (RSDs; Ross et al. 2007; Guzzo et al. 2008; Song & Percival 2009). Another wider application of the HLSS could be its abilities to conduct extensive plasma diagnostics and abundance analysis of rest-frame optical and UV emission lines from galaxies at cosmic noon ($z \sim 2$–3). In particular, optical emission lines such as [O III] $\lambda$5007, H$\alpha$ $\lambda$6563, [N II] $\lambda$6584, and UV lines e.g. C III] $\lambda\lambda$1907,1909 and O III] $\lambda\lambda$1661,1666 doublets, C IV $\lambda\lambda$1548,1551, and He II $\lambda$1640 lines in the rest frame of galaxies shifted to the near-IR windows provide unique insights into the metal enrichment in distant galaxies (see e.g., Erb et al. 2010; Leitherer et al. 2011; Stark et al. 2014, 2015; Rigby et al. 2015; Stark et al. 2017). These emission lines across a wider range of ionization levels, as shown in Fig. 2, can be used to track O/H, N/H, C/H, and ionization conditions of large populations of galaxies (see e.g., Jaskot & Ravindranath 2016; Pérez-Montero & Amorín 2017). Optical and UV emission-line analysis of galaxies at cosmic noon can enhance our understanding of the evolution of heavy elements in galaxies over cosmic time.

The HLSS is capable of measuring H$\alpha$ emission line redshifted to the range of $1.1 < z < 1.8$ observed with the WFI in the wavelength range of 1.38 to 1.85 $\mu$m. It can also be used to measure the [O III] $\lambda$5007 emission line within the range of $1.8 < z < 2.8$. Galaxy redshift surveys in grism spectroscopy require the detection of at least two emission lines, which can be implemented with H$\alpha$ $\lambda$6563 and [O III] $\lambda$5007 over the redshift range of 1.1 to 1.8. The ground-based observation have the capability to easily perform redshift surveys up to $z \sim 1$. Therefore, the *Roman* HLSS allows us to conduct redshift surveys of over 10 million galaxies at $z = 1.1$–$1.8$. The HLSS places strong constraints on H$\alpha$ $\lambda$6563 and [O III] $\lambda$5007 of various types of galaxies up to the redshift of 1.9. The *Roman* provides us with a greater number of galaxies, i.e. increasing the redshift survey's depth required for precise redshift-space distortions and robust constraints on the accelerating expansion of the universe emerged just after $z \sim 1.5$.

## 3 High Latitude Spectroscopic Survey: Emission-line Diagnostics

It is anticipated that the early stars in the nascent universe would exhibit remarkable dissimilarities to the stars in our immediate vicinity, primarily due to the non-existence of carbon, nitrogen, and oxygen elements (for further details, refer to Bromm 2013; Glover 2013; Greif 2015). The first generation stars, referred to as 'Population III,' possessed considerable mass of around $100 M_\odot$ (Abel et al. 2002; Schneider et al. 2002; Bromm et al. 2002; Bromm & Larson 2004) and exhibited $T_{\rm eff} \sim 10^5$ K (Bromm et al. 2001; Schaerer 2002). These stars were predominantly composed of hydrogen and helium. It is widely believed that Population III stars were responsible for the emergence of light at the end of the dark ages as well as the formation of carbon, nitrogen, and oxygen. This, in turn, facilitated the creation of the second generation of stars, known as "Population II" stars (Ostriker & Gnedin 1996; Heger & Woosley 2002), and first described by Burbidge et al. (1957). The shift from Pop III to Pop II is a significant occurrence in the cosmos that im-

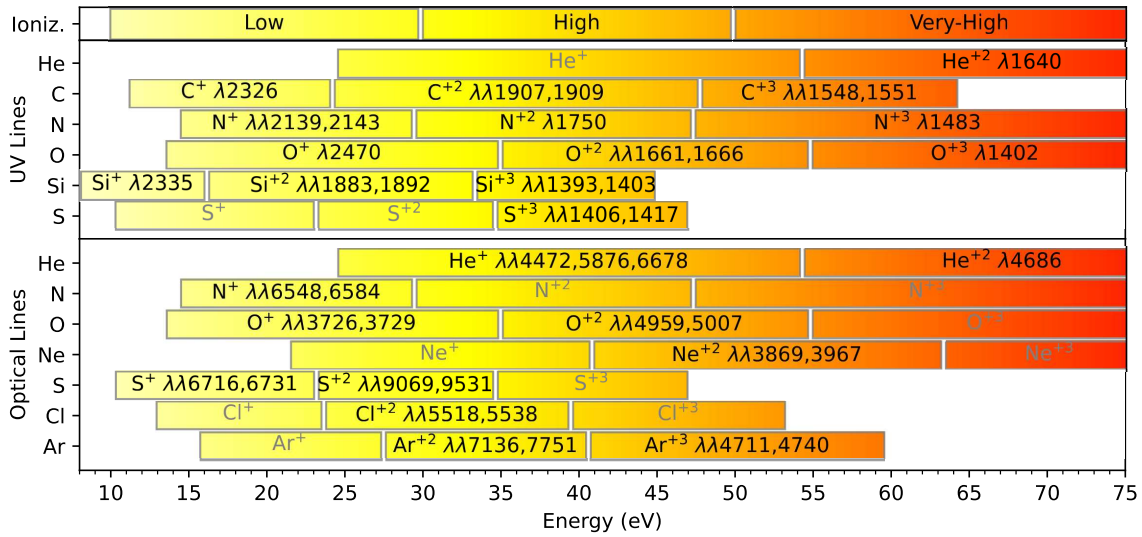


**Figure 2:** UV and optical emission lines observed in nebular structures of galaxies. The ions detectable in both the rest-frame UV and optical domains are placed on the top and bottom panels with their respective wavelengths across a broad range of ionization levels, repetitively. Various ionization levels are highlighted by a color gradient ranging from the yellow (low) to the red color (very-high ionization).

pacts the chemical make-up of stars and galaxies, and plays a role in the creation of molecular and dust during the early stages of the universe (Nozawa et al. 2003; Valiante et al. 2009; Gall et al. 2011; Leśniewska & Michałowski 2019). A fundamental inquiry in modern astronomy pertains to the temporal and causal factors underlying the emergence of enrichment in heavy elements after the epoch of reionization. Numerous spectroscopic investigations have been carried out recently to expound on the augmentation of metals and dust during the epoch of reionization (see, e.g. Hashimoto et al. 2019b,a; Liu & Hirashita 2019; Matthee et al. 2019; Tamura et al. 2019). The measurements of optical diagnostic lines, including [O III], H$\alpha$, [N II] $\lambda$6584, as well as UV lines such as C III] $\lambda$1908, O III] $\lambda$1664, C IV $\lambda$1548, and He II $\lambda$1640, facilitated by the *Roman* HLLS, as spectra of galaxies at cosmic noon are shifted to the near-IR window of the *Roman*, offer exceptional opportunity to determine the metal enrichment of distant galaxies as shown by previous works (e.g., Shapley et al. 2003; Erb et al. 2010; Leitherer et al. 2011; Stark et al. 2014; Rigby et al. 2015). The rest-frame optical and UV lines resolved with the HLLS have the potential to be employed for the purpose of deriving helium, oxygen, carbon, and nitrogen abundances (e.g., Danehkar et al. 2013; Danehkar 2021; Danehkar & Parthasarathy 2022), as well as the ionization states using photoionization modeling (e.g., Danehkar et al. 2014; Jaskot & Ravindranath 2016; Pérez-Montero & Amorín 2017; Danehkar 2018). Moreover, the optical lines such as [S II] $\lambda$6724, [O III] $\lambda$5007, H$\alpha$ $\lambda$6563, and H$\beta$ $\lambda$4861 can be used to distinguish star-forming and active galaxies (Kewley et al. 2001, 2006) via the so-called "BPT diagrams". It has also been demonstrated that UV diagnostic diagrams, built on the C IV $\lambda$1548, He II $\lambda$1640, O III] $\lambda$1664, and C III] $\lambda$1908 emission lines, are capable of distinguishing between active and starburst galaxies (Feltre et al. 2016; Gutkin et al. 2016). Moreover, these lines can provide valuable information about kinematics of stellar feedback (see, e.g., Danehkar 2015; Danehkar et al. 2016, 2018, 2021; Danehkar 2022) and non-equilibrium radiative effects (Gray et al. 2019; Danehkar et al. 2021, 2022). Hence, the analysis of the emission lines in the optical and UV spectra of galaxies will contribute to our

comprehension of the enrichment and evolution of chemical elements in star-forming and active galaxies throughout the history of the universe.

Several studies have provided compelling evidence indicating a decrease in star formation within starburst galaxies following cosmic reionization, which eventually led to its suppression in quiescent galaxies at cosmic noon (Birnboim et al. 2007; Kriek et al. 2007, 2008, 2011; Muzzin et al. 2013; Feldmann et al. 2017; Straatman et al. 2016). The number of quiescent galaxies with no star formation activity has recently been significantly increased within the redshift range of $1 < z < 4$ (Gobat et al. 2012; Straatman et al. 2016; Glazebrook et al. 2017; Cecchi et al. 2019; Belli et al. 2019). The identification of quiescent galaxies has been achieved through various methods such as EW(H$\beta$)–sSFR diagram (Wu et al. 2018) based on the fiducial-specific star-formation rate (sSFR$\equiv$ SFR$/M_\star$) and the equivalent width (EW) of H$\beta$. Various mechanisms have been proposed to suppress star formation in quiescent galaxies, including cool molecular winds from starburst regions (Bolatto et al. 2013), radiative feedback from young massive stars (Pawlik et al. 2013), supernova feedback (Stinson et al. 2007), UV photoheating (Hoeft et al. 2006; Dawoodbhoy et al. 2018), morphological effects (Martig et al. 2009; Bell et al. 2012), and strong mechanical feedback from supermassive black holes (Page et al. 2012; Alatalo et al. 2015; Wylezalek & Zakamska 2016). In addition, certain physical factors present in host galaxies may play a role in inhibiting the process of star formation. These factors include but are not limited to metallicity (Krumholz & Dekel 2012), galactic outflows (Cano-Díaz et al. 2012; Balmaverde et al. 2016), dense media (Tran et al. 2010; Quadri et al. 2012; Fang et al. 2013), turbulence contributions (Lanz et al. 2016). Therefore, the determination of chemical and physical properties through diagnostics of optical and UV emission lines measured in galaxies during the cosmic noon period using the *Roman* HLSS will yield new perspectives on the underlying physical mechanisms and evolutionary channels that result in the regulation of star formation in galaxies across cosmic time.

## 4 *Roman* Grism Spectroscopic Surveys of Galaxies at Cosmic Noon

The slitless grism WFI on the *Roman* will facilitate extensive near-IR spectroscopic analysis across a broad area of observation. Recently, *Roman* grism simulations have demonstrated that a comprehensive survey using deep *Roman* grism observations can effectively measure the Ly$\alpha$ emission (Wold et al. 2023). The Ly$\alpha$ measurements can be used to deduce the ionization states of high-$z$ galaxies and examine various models of reionization. The use of slitless grism capabilities is highly appropriate for space telescopes, where the sky background is insignificant. In such a case, slitless modes are the most straightforward approach to incorporating spectroscopy into a mission. In addition, it is noteworthy that slitless observations exhibit high efficiency in conducting spectroscopic surveys, owing to the fact that the light of all objects present within the field of view is dispersed across the detector. This attribute is notably advantageous in resolving emission-line fluxes that may not be detected in slit-mask observations owing to the bright continuum.

Recently, Wold et al. (2023) presented a pioneering method of data cube search for *Roman* grism data extraction, named "CUBGRISM", which was initially designed for GALEX grism data. Their main aim was to evaluate the efficacy of resolving Ly$\alpha$ emitters (LAEs) with the *Roman* grism spectroscopy. The CUBGRISM does not require a wide-ranging detection and was devised to generate a sample of datacube fluxes, which are suited for characterizing LAEs through *Roman* grism deep field observations. The CUBGRISM technique (described in details by Barger et al. 2012; Wold et al. 2014, 2017) involves the transformation of several slitless spectroscopic

images into a 3D datacube, namely two spatial axes and one wavelength axis. *Roman* grism simulations of the Ly$\alpha$ emission provided a datacube with a wavelength increment of 10 Å and a wavelength span of roughly 1.0-1.5 $\mu$m (Wold et al. 2023). However, their wavelength range were intentionally chosen to cover the wavelength domain and spectral resolution of the *Roman* with the purpose of measuring high-$z$ LAEs ($z = 7.5$–$10.5$), so they imposed an artificial constraint on the wavelength range of the resultant datacube. Future extended simulations are necessary for covering the rest-frame UV and optical lines redshifted into the near-IR grism window (1.0–1.93 $\mu$m). The currently simulated *Roman* datacubes over 1–1.49 $\mu$m allows the evaluation of LAEs of $z = 7.24$–$11.25$. Applying SExtractor (Bertin & Arnouts 1996) to each wavelength slice, Wold et al. (2023) demonstrated that *Roman* Grism spectroscopy is capable of identifying Ly$\alpha$ datacube flux with a significance level above 7.5$\sigma$ that can mitigate the occurrence of erroneous detection within the cube.

The applicability of CUBGRISM to Roman grism data, as shown by Wold et al. (2023), can be employed to generate a emission-line flux-limited sample required for diagnostics of the rest-frame optical and UV emission lines measured in galaxies at $1 < z < 2$. The CUBGRISM results suggest that emission-line diagnostics using a deep *Roman* grism has the potential to attain optical and UV emission-line depths that are suitable for the determination of physical conditions and elemental abundances of ionized gaseous nebulae and H II regions within galaxies over $z \sim 1$–$2$. This would enable us to trace metallicity, ionizing fields, stellar populations, star formation rates, kinematics of stellar feedback, and the ionization condition of the ISM within active and star-forming galaxies at cosmic noon.

## References


Abel, T., Bryan, G. L., & Norman, M. L. 2002, Science, 295, 93
Alatalo, K., Lacy, M., Lanz, L., et al. 2015, ApJ, 798, 31
Bagley, M. B., Scarlata, C., Henry, A., et al. 2017, ApJ, 837, 11
Balmaverde, B., Marconi, A., Brusa, M., et al. 2016, A&A, 585, A148
Balzano, V. A. 1983, ApJ, 268, 602
Barger, A. J., Cowie, L. L., & Wold, I. G. B. 2012, ApJ, 749, 106
Becker, G. D., Bolton, J. S., Madau, P., et al. 2015, MNRAS, 447, 3402
Beckwith, S. V. W., Stiavelli, M., Koekemoer, A. M., et al. 2006, AJ, 132, 1729
Bell, E. F., van der Wel, A., Papovich, C., et al. 2012, ApJ, 753, 167
Belli, S., Newman, A. B., & Ellis, R. S. 2019, ApJ, 874, 17
Bertin, E. & Arnouts, S. 1996, A&AS, 117, 393
Birnboim, Y., Dekel, A., & Neistein, E. 2007, MNRAS, 380, 339
Bolatto, A. D., Warren, S. R., Leroy, A. K., et al. 2013, Nature, 499, 450
Bouwens, R. J., Illingworth, G. D., Oesch, P. A., et al. 2014, ApJ, 793, 115
Bromm, V. 2013, Rept. Prog. Phys., 76, 112901
Bromm, V., Coppi, P. S., & Larson, R. B. 2002, ApJ, 564, 23
Bromm, V., Kudritzki, R. P., & Loeb, A. 2001, ApJ, 552, 464
Bromm, V. & Larson, R. B. 2004, ARA&A, 42, 79
Burbidge, E. M., Burbidge, G. R., Fowler, W. A., & Hoyle, F. 1957, Rev. Mod. Phys., 29, 547
Caldwell, R. R. & Kamionkowski, M. 2009, Annu. Rev. Nucl. Part. Sci., 59, 397
Cano-Díaz, M., Maiolino, R., Marconi, A., et al. 2012, A&A, 537, L8
Cecchi, R., Bolzonella, M., Cimatti, A., & Girelli, G. 2019, ApJ, 880, L14
Curtis-Lake, E., McLure, R. J., Dunlop, J. S., et al. 2016, MNRAS, 457, 440
Danehkar, A. 2015, ApJ, 815, 35
Danehkar, A. 2018, PASA, 35, e005
Danehkar, A. 2021, ApJS, 257, 58

Danehkar, A. 2022, ApJS, 260, 14
Danehkar, A., Karovska, M., Maksym, W. P., & Montez, Rodolfo, J. 2018, ApJ, 852, 87
Danehkar, A., Oey, M. S., & Gray, W. J. 2021, ApJ, 921, 91
Danehkar, A., Oey, M. S., & Gray, W. J. 2022, ApJ, 937, 68
Danehkar, A., Parker, Q. A., & Ercolano, B. 2013, MNRAS, 434, 1513
Danehkar, A., Parker, Q. A., & Steffen, W. 2016, AJ, 151, 38
Danehkar, A. & Parthasarathy, M. 2022, MNRAS, 514, 1217
Danehkar, A., Todt, H., Ercolano, B., & Kniazev, A. Y. 2014, MNRAS, 439, 3605
Dawoodbhoy, T., Shapiro, P. R., Ocvirk, P., et al. 2018, MNRAS, 480, 1740
Dijkstra, M. 2014, PASA, 31, e040
Drakos, N. E., Villasenor, B., Robertson, B. E., et al. 2022, ApJ, 926, 194
Ellis, R. S., McLure, R. J., Dunlop, J. S., et al. 2013, ApJ, 763, L7
Erb, D. K., Pettini, M., Shapley, A. E., et al. 2010, ApJ, 719, 1168
Fang, J. J., Faber, S. M., Koo, D. C., & Dekel, A. 2013, ApJ, 776, 63
Feldmann, R., Hopkins, P. F., Quataert, E., Faucher-Giguère, C.-A., & Kereš, D. 2016, MNRAS, 458, L14
Feldmann, R., Quataert, E., Hopkins, P. F., Faucher-Giguère, C.-A., & Kereš, D. 2017, MNRAS, 470, 1050
Feltre, A., Charlot, S., & Gutkin, J. 2016, MNRAS, 456, 3354
Finkelstein, S. L., Papovich, C., Ryan, R. E., et al. 2012, ApJ, 758, 93
Finkelstein, S. L., Ryan, Russell E., J., Papovich, C., et al. 2015, ApJ, 810, 71
Frieman, J. A., Turner, M. S., & Huterer, D. 2008, ARA&A, 46, 385
Gall, C., Hjorth, J., & Andersen, A. C. 2011, A&A Rev., 19, 43
Giavalisco, M. 2002, ARA&A, 40, 579
Giavalisco, M., Ferguson, H. C., Koekemoer, A. M., et al. 2004, ApJ, 600, L93
Glazebrook, K., Schreiber, C., Labbé, I., et al. 2017, Nature, 544, 71
Glover, S. 2013, in ASSL, Vol. 396, The First Galaxies, ed. T. Wiklind, B. Mobasher, & V. Bromm, 103
Gobat, R., Strazzullo, V., Daddi, E., et al. 2012, ApJ, 759, L44
Gómez-Guijarro, C., Toft, S., Karim, A., et al. 2018, ApJ, 856, 121
González Delgado, R. M., Heckman, T., Leitherer, C., et al. 1998, ApJ, 505, 174
Gray, W. J., Oey, M. S., Silich, S., & Scannapieco, E. 2019, ApJ, 887, 161
Greif, T. H. 2015, Comput. Astrophys. Cosmol., 2, 3
Grogin, N. A., Kocevski, D. D., Faber, S. M., et al. 2011, ApJS, 197, 35
Gutkin, J., Charlot, S., & Bruzual, G. 2016, MNRAS, 462, 1757
Guzzo, L., Pierleoni, M., Meneux, B., et al. 2008, Nature, 451, 541
Hashimoto, T., Inoue, A. K., Mawatari, K., et al. 2019a, PASJ, 71, 71
Hashimoto, T., Inoue, A. K., Tamura, Y., et al. 2019b, PASJ, 71, 109
Hayes, M. 2015, PASA, 32, e027
Heckman, T. M., González-Delgado, R., Leitherer, C., et al. 1997, ApJ, 482, 114
Heger, A. & Woosley, S. E. 2002, ApJ, 567, 532
Hoeft, M., Yepes, G., Gottlöber, S., & Springel, V. 2006, MNRAS, 371, 401
Illingworth, G. D., Magee, D., Oesch, P. A., et al. 2013, ApJS, 209, 6
Jaskot, A. E. & Ravindranath, S. 2016, ApJ, 833, 136
Kawamata, R., Oguri, M., Ishigaki, M., Shimasaku, K., & Ouchi, M. 2016, ApJ, 819, 114
Kewley, L. J., Dopita, M. A., Sutherland, R. S., Heisler, C. A., & Trevena, J. 2001, ApJ, 556, 121
Kewley, L. J., Groves, B., Kauffmann, G., & Heckman, T. 2006, MNRAS, 372, 961
Koekemoer, A. M., Aussel, H., Calzetti, D., et al. 2007, ApJS, 172, 196
Koekemoer, A. M., Ellis, R. S., McLure, R. J., et al. 2013, ApJS, 209, 3
Koekemoer, A. M., Faber, S. M., Ferguson, H. C., et al. 2011, ApJS, 197, 36
Kriek, M., van der Wel, A., van Dokkum, P. G., Franx, M., & Illingworth, G. D. 2008, ApJ, 682, 896
Kriek, M., van Dokkum, P. G., Franx, M., et al. 2007, ApJ, 669, 776
Kriek, M., van Dokkum, P. G., Whitaker, K. E., et al. 2011, ApJ, 743, 168
Krumholz, M. R. & Dekel, A. 2012, ApJ, 753, 16
Lanz, L., Ogle, P. M., Alatalo, K., & Appleton, P. N. 2016, ApJ, 826, 29
Leitherer, C., Tremonti, C. A., Heckman, T. M., & Calzetti, D. 2011, AJ, 141, 37
Leśniewska, A. & Michałowski, M. J. 2019, A&A, 624, L13

Limousin, M., Richard, J., Jullo, E., et al. 2016, A&A, 588, A99
Liu, H.-M. & Hirashita, H. 2019, MNRAS, 490, 540
Lotz, J. M., Koekemoer, A., Coe, D., et al. 2017, ApJ, 837, 97
Mahler, G., Richard, J., Clément, B., et al. 2018, MNRAS, 473, 663
Martig, M., Bournaud, F., Teyssier, R., & Dekel, A. 2009, ApJ, 707, 250
Matthee, J., Sobral, D., Boogaard, L. A., et al. 2019, ApJ, 881, 124
Muzzin, A., Marchesini, D., Stefanon, M., et al. 2013, ApJ, 777, 18
Nozawa, T., Kozasa, T., Umeda, H., Maeda, K., & Nomoto, K. 2003, ApJ, 598, 785
Oesch, P. A., Bouwens, R. J., Illingworth, G. D., et al. 2010, ApJ, 709, L16
Oesch, P. A., Bouwens, R. J., Illingworth, G. D., et al. 2013, ApJ, 773, 75
Oesch, P. A., Bouwens, R. J., Illingworth, G. D., Labbé, I., & Stefanon, M. 2018, ApJ, 855, 105
Oesch, P. A., Stiavelli, M., Carollo, C. M., et al. 2007, ApJ, 671, 1212
Ono, Y., Ouchi, M., Curtis-Lake, E., et al. 2013, ApJ, 777, 155
Ostriker, J. P. & Gnedin, N. Y. 1996, ApJ, 472, L63
Page, M. J., Symeonidis, M., Vieira, J. D., et al. 2012, Nature, 485, 213
Pawlik, A. H., Milosavljević, M., & Bromm, V. 2013, ApJ, 767, 59
Pérez-Montero, E. & Amorín, R. 2017, MNRAS, 467, 1287
Priewe, J., Williams, L. L. R., Liesenborgs, J., Coe, D., & Rodney, S. A. 2017, MNRAS, 465, 1030
Quadri, R. F., Williams, R. J., Franx, M., & Hildebrandt, H. 2012, ApJ, 744, 88
Rafelski, M., Teplitz, H. I., Gardner, J. P., et al. 2015, AJ, 150, 31
Richard, J., Pelló, R., Schaerer, D., Le Borgne, J. F., & Kneib, J. P. 2006, A&A, 456, 861
Rieke, G. H., Lebofsky, M. J., Thompson, R. I., Low, F. J., & Tokunaga, A. T. 1980, ApJ, 238, 24
Rigby, J. R., Bayliss, M. B., Gladders, M. D., et al. 2015, ApJ, 814, L6
Robertson, B. E., Furlanetto, S. R., Schneider, E., et al. 2013, ApJ, 768, 71
Ross, N. P., da Ângela, J., Shanks, T., et al. 2007, MNRAS, 381, 573
Rutkowski, M. J., Scarlata, C., Haardt, F., et al. 2016, ApJ, 819, 81
Schaerer, D. 2002, A&A, 382, 28
Schneider, R., Ferrara, A., Natarajan, P., & Omukai, K. 2002, ApJ, 571, 30
Scoville, N., Abraham, R. G., Aussel, H., et al. 2007, ApJS, 172, 38
Shapley, A. E., Steidel, C. C., Pettini, M., & Adelberger, K. L. 2003, ApJ, 588, 65
Song, Y.-S. & Percival, W. J. 2009, J. Cosmol. Astropart. Phys., 2009, 004
Stark, D. P., Ellis, R. S., Charlot, S., et al. 2017, MNRAS, 464, 469
Stark, D. P., Richard, J., Siana, B., et al. 2014, MNRAS, 445, 3200
Stark, D. P., Walth, G., Charlot, S., et al. 2015, MNRAS, 454, 1393
Stinson, G. S., Dalcanton, J. J., Quinn, T., Kaufmann, T., & Wadsley, J. 2007, ApJ, 667, 170
Straatman, C. M. S., Spitler, L. R., Quadri, R. F., et al. 2016, ApJ, 830, 51
Tamura, Y., Mawatari, K., Hashimoto, T., et al. 2019, ApJ, 874, 27
Teplitz, H. I., Rafelski, M., Kurczynski, P., et al. 2013, AJ, 146, 159
Tilvi, V., Papovich, C., Finkelstein, S. L., et al. 2014, ApJ, 794, 5
Tran, K.-V. H., Papovich, C., Saintonge, A., et al. 2010, ApJ, 719, L126
Trenti, M., Stiavelli, M., Bouwens, R. J., et al. 2010, ApJ, 714, L202
Troxel, M. A., Long, H., Hirata, C. M., et al. 2021, MNRAS, 501, 2044
Valiante, R., Schneider, R., Bianchi, S., & Andersen, A. C. 2009, MNRAS, 397, 1661
Vega-Ferrero, J., Diego, J. M., & Bernstein, G. M. 2019, MNRAS, 486, 5414
Wang, Y., Zhai, Z., Alavi, A., et al. 2022, ApJ, 928, 1
Weedman, D. W., Feldman, F. R., Balzano, V. A., et al. 1981, ApJ, 248, 105
Weinberg, D. H., Mortonson, M. J., Eisenstein, D. J., et al. 2013, Phys. Rep., 530, 87
Wold, I. G. B., Barger, A. J., & Cowie, L. L. 2014, ApJ, 783, 119
Wold, I. G. B., Finkelstein, S. L., Barger, A. J., Cowie, L. L., & Rosenwasser, B. 2017, ApJ, 848, 108
Wold, I. G. B., Malhotra, S., Rhoads, J. E., Tilvi, V., & Gabrielpillai, A. 2023, arXiv e-prints, arXiv:2305.01562
Wu, P.-F., van der Wel, A., Bezanson, R., et al. 2018, ApJ, 868, 37
Wylezalek, D. & Zakamska, N. L. 2016, MNRAS, 461, 3724
Yamamoto, M., Troxel, M. A., Jarvis, M., et al. 2023, MNRAS, 519, 4241